Petroleum Science 21 (2024) 458–474

Contents lists available at ScienceDirect

Petroleum Science

journal homepage: www.keaipublishing.com/en/journals/petroleum-science

Original Paper

Prediction models of burst strength degradation for casing with considerations of both wear and corrosion

Jie-Li Wang [a, b], Wen-Jun Huang [a, b, *], De-Li Gao [a, b, *]

[a] MOE Key Laboratory of Petroleum Engineering, China University of Petroleum, Beijing, 102249, China
[b] State Key Laboratory of Petroleum Resources and Prospecting, China University of Petroleum, Beijing, 102249, China

ARTICLE INFO

Article history:
Received 24 November 2022
Received in revised form
27 April 2023
Accepted 9 August 2023
Available online 10 August 2023

Edited by Jia-Jia Fei

Keywords:
Deep well
Casing integrity
Casing wear
Casing corrosion
Burst strength

ABSTRACT

Casing wear and casing corrosion are serious problems affecting casing integrity failure in deep and ultra-deep wells. This paper aims to predict the casing burst strength with considerations of both wear and corrosion. Firstly, the crescent wear shape is simplified into three categories according to common mathematical models. Then, based on the mechano-electrochemical (M-E) interaction, the prediction model of corrosion depth is built with worn depth as the initial condition, and the prediction models of burst strength of the worn casing and corroded casing are obtained. Secondly, the accuracy of different prediction models is validated by numerical simulation, and the main influence factors on casing strength are obtained. At last, the theoretical models are applied to an ultra-deep well in Northwest China, and the dangerous well sections caused by wear and corrosion are predicted, and the corrosion rate threshold to ensure the safety of casing is obtained. The results show that the existence of wear defects results in a stress concentration and enhanced M-E interaction on corrosion depth growth. The accuracy of different mathematical models is different: the slot ring model is most accurate for predicting corrosion depth, and the eccentric model is most accurate for predicting the burst strength of corroded casing. The burst strength of the casing will be overestimated by more than one-third if the M-E interaction is neglected, so the coupling effect of wear and corrosion should be sufficiently considered in casing integrity evaluation.
© 2023 The Authors. Publishing services by Elsevier B.V. on behalf of KeAi Communications Co. Ltd. This is an open access article under the CC BY-NC-ND license (http://creativecommons.org/licenses/by-nc-nd/4.0/).

1. Introduction

Casing integrity is an important assurance for safe drilling and well operations. As the increase of well depth, long drilling periods and complex down-hole conditions lead to serious casing wear. On the other hand, acid gas is contained in many oil and gas wells, and casing corrosion is inevitable (Zhu and Liu, 2018). Especially for deep and ultra-deep wells, casing failure problems due to serious wear and corrosion occur frequently. Therefore, accurate prediction of the casing corrosion depth as well as the residual strength of casing is very important for safe operation.

A lot of studies on casing wear and casing corrosion have been carried out from various perspectives. White and Dawson (1987) established a linear wear efficiency model to predict the casing wear depth. This model is verified by theoretical identification and field testing, and many subsequent researches for casing wear prediction have been done on this wear mechanism (Chu et al., 2009; Gao et al., 2010; Huang et al., 2021). To analyze the effects of casing wear on casing strength degradation, different methods were conducted. Wang et al. (2013) verified the reliability of the finite element algorithm through a full-scale test of worn casing, and analyzed the influence of different factors on casing residual strength. Zhang et al. (2020) studied the calculation models of worn casing and indicated that the crescent-shaped wear model is more accurate for the residual burst strength prediction of worn casing. Jin et al. (2020) derived the casing collapse strength formula considering compound sharp wear and compound blunt wear. Teigland et al. (2021) analyzed the stress distribution of crescent-shaped worn casing by the finite element method and obtained the empirical expressions for stress concentration.

Corrosion is another important reason for the strength degradation of casing (Qin and Cheng, 2021; Qian and Cheng, 2019; Liu

* Corresponding author. MOE Key Laboratory of Petroleum Engineering, China University of Petroleum, Beijing 102249, China.
E-mail addresses: huangwenjun1986@126.com (W.-J. Huang), gaodeli_team@126.com (D.-L. Gao).

https://doi.org/10.1016/j.petsci.2023.08.014
1995-8226/© 2023 The Authors. Publishing services by Elsevier B.V. on behalf of KeAi Communications Co. Ltd. This is an open access article under the CC BY-NC-ND license (http://creativecommons.org/licenses/by-nc-nd/4.0/).

et al., 2019). Hou et al. (2013) studied the degradation of casing steel mechanical properties in sour environments by using tensile and impact tests. Lin et al. (2016) conducted the casing wear and corrosion experiments and calculated the residual strength of the casing after wear and corrosion. Chen et al. (2017) proposed a burst pressure equation for corroded pipes and validated the accuracy of the equation with experimental data. Zhang et al. (2018) conducted a high temperature high pressure flow corrosion test and proposed the finite service life evaluation method for corroded casing. Yan et al. (2019) established a numerical model of the casing with double ellipsoidal corrosion pits and analyzed the residual strength of casing under different conditions. Chen et al. (2020) proposed that the corrosion defects would reduce the residual strength of the tubing with the effect of frost heaving force. Chen et al. (2021) and Zeng et al. (2021) studied the corrosion behavior of casing steel by corrosion tests and calculated the residual strength of corroded casing by numerical simulation. Zhang and Zhou (2021) proposed a burst capacity model for corroded pipelines considering the width and length of corrosion defects.

As mentioned above, a lot of attention has been paid to the casing wear and casing corrosion. However, the research on casing wear and casing corrosion is relatively independent, and the majority of the studies did not consider the effect of stress on corrosion process. It has been demonstrated that stress can accelerate corrosion and lead to the early failure of engineering structures (Yang et al., 2016; Wang et al., 2021). There are some studies involving damage evolution, where the mechanical-electrochemical (M-E) interaction is considered. The M-E interaction model was first proposed by Gutman (1994) and has been applied to the residual strength degradation of engineering structures in corrosive environments, such as oil and gas pipelines, marine risers, and casing pipes. Sun and Cheng (2019, 2020) developed a finite element model to simulate and determine the M-E interaction at overlapped corrosion defects on an X46 steel pipeline, and compared the finite element results with the theoretical model proposed by Gutman (1994). The results show that the variations between the theoretical calculations and the modeling results are less than 10%. The materials and service conditions of the casing pipes and pipelines are similar. They all belong to high-strength steel and pass through complex underground conditions. In addition to the hoop stress induced by internal pressure, they also suffer from severe corrosion. Therefore, this theory is also applied to the prediction of failure pressure and service life of corroded casing (Zhang et al., 2017). In previous studies, the wellbore environment is not as critical as that of ultra-deep wells, and the effect of casing wear is not fully considered. In other words, the coupling effect of casing wear and corrosion is not studied systematically.

In this study, the coupling effect between casing wear and corrosion is studied, in which the mechanical-electrochemical interaction on damage evolution is considered. The theoretical models are established to calculate the corrosion depth and the burst strength of the corroded casing. Next, theoretical models are verified by numerical simulations, and the influence of main factors on burst strength is discussed. Finally, a case study of casing corrosion prediction and residual strength calculation is conducted for an ultra-deep well.

1.1. Structure of this paper

In this paper, an analytical method is used to study the coupling effect of wear and corrosion on casing burst strength. First, the prediction model of casing corrosion depth is built with the worn depth as the initial condition, and the prediction model of burst strengths of the worn and corrosion casings is obtained in section 2. Next, numerical simulations are conducted to validate the prediction models of casing corrosion depth and burst strength in section 3. At last, the theoretical models are applied to an ultra-deep well in section 4. To facilitate the understanding of the logical relationship among various parts, the main structure of this paper is shown in Fig. 1.

2. Theoretical models

2.1. Casing wear and corrosion process

A schematic plot of casing wear and corrosion in a deep well is shown in Fig. 2. With the increase of well depth, the wear time between the drill string and casing increases, resulting in the increase of wear depth. As shown in Fig. 2(a)–(b), the worn area on casing is like a crescent. During the subsequent operations, the worn casing is inevitably exposed to a corrosive environment, and the inner wall of the casing is further corroded, as shown in Fig. 2(c)–(d). With the increase of the effects of wear and corrosion, the casing wall becomes thinner, resulting in a more significant degradation of casing strength.

This paper focuses on the casing corrosion problem in which the casing wear shape is taken as the initial condition. Section 2.2 builds the prediction model of casing corrosion depth in which the entire corrosion process can be viewed as the cumulation of a series of sub-processes, and the corrosion depth is equal to the product of corrosion rate and time increment in every sub-process. Section 2.3 presents the prediction model of the casing burst strength with consideration of both wear and corrosion.

2.2. Prediction model of casing corrosion depth

In the casing corrosion system, the casing is subjected to corrosion solution and fluid pressure. According to the mechanical-electrochemical interaction, the thermodynamic activity and electrochemical reaction potential of the casing will be changed. In addition, the casing wear leads to local stress concentration, which makes the corrosion potential lower, the corrosion current density larger, and the corrosion rate faster. The change process of mechano-electrochemical activity and equilibrium potential of the casing corrosion system is shown in Appendix A. As shown in Eq. (1), based on the mass action law and electric charge equilibrium equation, Gutman (1994) obtained the relationship between metal dissolution current I and pressure ΔP.

$$I = i_a \exp\frac{\Delta PV}{R(T+273.15)} - i_k \tag{1}$$

where I is the metal dissolution current; i_a is the anode current of undeformed electrode; i_k is the cathode current; ΔP is the residual pressure in MPa; R is the general gas constant in J/(mol·K); T is the temperature in °C; V is the molar volume of casing in m^3/mol.

As can be seen from Eq. (1), when the metal is dissolved, only the anode current depends on the mechanical effect, while the cathode current is independent of it. The influence coefficient of stress on anode current is approximated as its influence coefficient on corrosion rate, and the relationship between corrosion rate and stress is obtained.

$$V_t = V_o \exp\frac{V\sigma_\theta}{RT} \tag{2}$$

where V_t is the accelerated corrosion rate in mm/y; V_o is the initial corrosion rate in mm/y; σ_θ is the hoop stress at time t in MPa.

The accumulated corrosion depth is calculated by

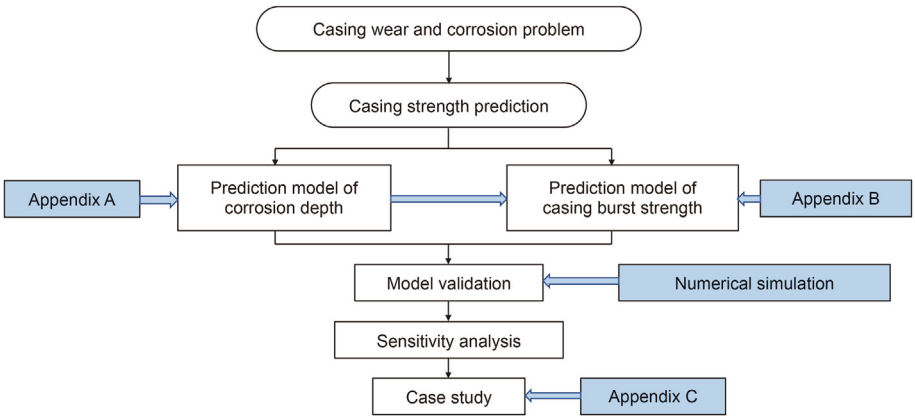

Fig. 1. Main structure of this paper.

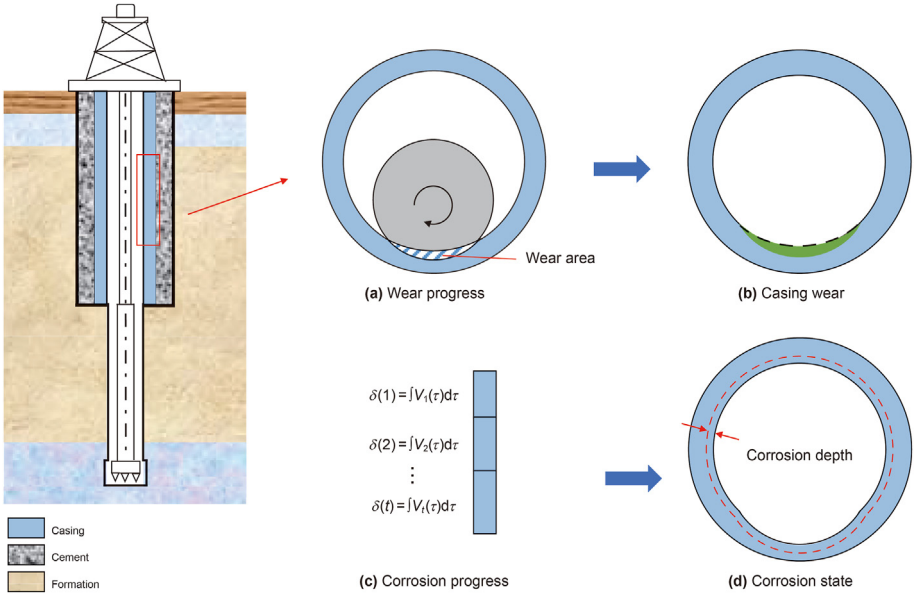

Fig. 2. A schematic plot of the wellbore.

$$\delta(t) = \int_0^t V_t(\tau)\mathrm{d}\tau \tag{3}$$

where t is the accumulated corrosion time; $\delta(t)$ is the accumulated corrosion depth in mm.

The remaining wall thickness of casing is expressed as

$$h = t_o - w - \delta(t) \tag{4}$$

where t_o is the initial wall thickness of casing in mm; w is the wear depth in mm; h is the remaining wall thickness of casing in mm.

Hoop stress of damaged casing. The stress state of the casing is shown in Fig. 3(a). The casing is filled with corrosive fluid and subjected to internal pressure from the fluid. According to the prediction model of casing corrosion depth, hoop stress is the key parameter to calculate the corrosion depth. When the casing is worn, it is difficult to obtain the theoretical expression of stress distribution near the worn area. To facilitate theoretical calculation, the crescent wear casing is usually simplified as a slotted model (Wu and Zhang, 2005), an eccentric model (Chen et al., 2017), and a uniform model. Here, the above simplified models of worn casing are expanded to corroded casings.

The slot ring model, as shown in Fig. 3(b), simplifies the damaged shape as a slot, where the wear depth is w and the corrosion depth is $\delta(t)$. As shown in Fig. 3(c), the eccentric model uses geometric eccentricity to depict the wear and corrosion shape. The outer radius and the center of the unworn casing are r_o and o_1, the circle with radius r and center o_2 represents the nominal inner wall of the eccentric pipe. The uniform model, as shown in Fig. 3(d), assumes a uniform thickness reduction around the casing inner wall. The circle with radius r represents the nominal inner wall of the uniform damaged model.

Based on the slot ring model, eccentric model, and uniform model, hoop stresses on casing considering wear and corrosion are deduced in Appendix B, and the hoop stresses are further introduced to Eq. (2) for corrosion rate calculation. In this way, the effect of casing stress is considered in corrosion depth prediction. The calculation expressions of hoop stresses for these three models are given as follows.

***For slot ring model*:** By considering the corrosion depth $\delta(t)$, the change of hoop stress is expressed as

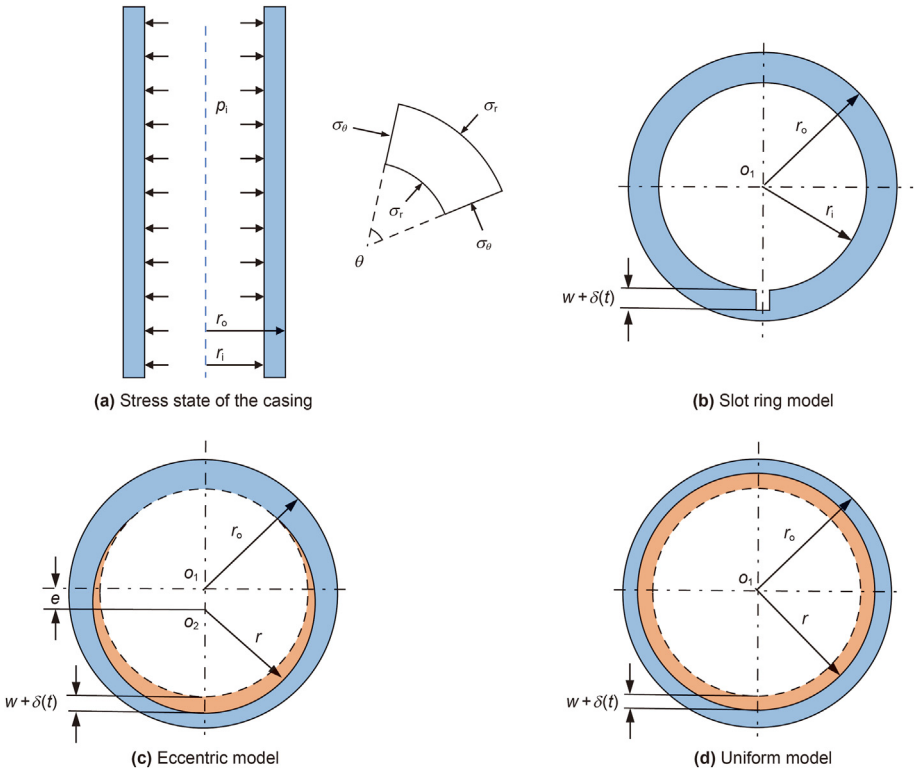

(a) Stress state of the casing (b) Slot ring model (c) Eccentric model (d) Uniform model

Fig. 3. The calculation model of the hoop stress considering corrosion and wear.

$$\sigma_{\theta,t}=\frac{p_i {r_i}^2}{{r_o}^2-{r_i}^2}+\frac{p_i {r_i}^2 {r_o}^2}{{r_o}^2-{r_i}^2}\frac{1}{r^2}+\frac{F}{t_o-w-\delta(t)}-\frac{1.95F(2r-r_o-r_i-w-\delta(t))}{(t_o-w-\delta(t))^2} \tag{5}$$

where

$$F=p_i(w+\delta(t))+\frac{p_i {r_i}^2}{{r_o}^2-{r_i}^2}(w+\delta(t))+\frac{p_i {r_i}^2 {r_o}^2}{{r_o}^2-{r_i}^2}\frac{(w+\delta(t))}{r_i(r_i+w+\delta(t))}$$

where $\sigma_{\theta,t}$ is the hoop stress of deepest point of the damaged casing in MPa; p_i is the internal pressure in MPa; t_o is the initial wall of casing in mm; r_o is the casing outer radius in mm; r_i is the casing inner radius in mm; r is the casing radial coordinate in mm, $r=r_i+w+\delta(t)$; w is the initial wear depth in mm; $\delta(t)$ is the corrosion depth in mm, F is the hoop force in N.

***For eccentric model*:** By considering the corrosion depth $\delta(t)$, the change of hoop stress is expressed as

$$\sigma_{\theta,t}=\frac{\left[({r_o}^2+r^2-e^2)^2({r_o}^2-r^2)+(2r-e)4r^2{r_o}^2e\right]p_i}{({r_o}^2+r^2)\left[({r_o}^2+r^2-e^2)^2-4r^2{r_o}^2\right]} \tag{6}$$

where $r=r_i+e=r_i+(w+\delta(t))/2$, e is the eccentric distance.

***For uniform model*:** By considering the corrosion depth $\delta(t)$, the change of hoop stress is expressed as

$$\sigma_{\theta,t}=\frac{p_i r}{h} \tag{7}$$

where $r=r_i+w+\delta(t)$, h is the remaining wall of the casing.

2.3. Prediction model of casing burst pressure

When the casing is worn, the casing wall thickness becomes thin, and casing strength decreases. The effect of casing corrosion on casing strength is similar to casing wear (Zhang et al., 2020). By combing the stress expression and the failure criterion, the prediction model of casing burst pressure considering both wear and corrosion is established. Here, the wear depth is the initial amount, and the corrosion depth is the damage evolution increment.

***For slot ring model*:** The failure criterion is the condition that the hoop stress in the middle of the remaining wall is equal to the yield strength. The casing burst pressure of the slot ring model is expressed as

$$p_b=\frac{\sigma_s}{f} \tag{8}$$

where

$$f=\frac{{r_i}^2}{{r_o}^2-{r_i}^2}+\frac{{r_i}^2{r_o}^2}{{r_o}^2-{r_i}^2}\frac{1}{{r_c}^2}+\frac{f_0}{t_o-w-\delta(t)}-\frac{1.95f_0(2r_c-r_o-r_i-w-\delta(t))}{(t_o-w-\delta(t))^2}$$

$$f_0=w+\delta(t)+\frac{{r_i}^2}{{r_o}^2-{r_i}^2}(w+\delta(t))+\frac{{r_i}^2{r_o}^2}{{r_o}^2-{r_i}^2}\frac{(w+\delta(t))}{r_i(r_i+w+\delta(t))}$$

where r_c is the radial position of the yield point in mm, $r_c=(r_i+r_o+w+\delta(t))/2$; σ_s is the yield strength of casing in MPa; p_b is the burst pressure in MPa; w is the wear depth of casing in mm; $\delta(t)$ is the corrosion depth of casing in mm; r_o is the outer radius of

casing in mm; r_i is the inner radius of casing in mm.

For eccentric model: The failure criterion is the condition that the hoop stress of the inner wall is equal to the yield strength (Lin et al., 2016). The casing burst pressure of eccentric model is expressed as

$$p_b = \frac{\sigma_s(r_o^2 + r_c^2)\left[(r_o^2 + r_c^2 - e^2)^2 - 4r_c^2 r_o^2\right]}{(r_o^2 + r_c^2 - e^2)^2(r_o^2 - r_c^2) + (2r - e)4r_c^2 r_o^2 e} \tag{9}$$

where $r_c = r_i + e = r_i + (w + \delta(t))/2$; p_b is the burst pressure in MPa.

For uniform model: The American Petroleum Institute (API) provided an equation for calculation of burst strength of pipe. By using the remaining casing wall to substitute into the API equation, the burst strength of worn casing is calculated. The formula to calculate the burst pressure is shown as Eq. (10), where the factor 0.875 accounts for the API pipe wall thickness tolerance of 12.5% less than the nominal wall thickness. The casing burst pressure of uniform model is expressed as

$$p_b = 0.875\left[\frac{\sigma_s(t_o - w - \delta(t))}{r_o}\right] \tag{10}$$

where p_b is the burst pressure of casing in MPa; t_o is the initial wall of casing in mm.

3. Model validation and sensitivity analysis

In order to verify the accuracy of the prediction model of corrosion depth and burst strength, the numerical simulation is carried out by using ANSYS software. In the analysis, TP140V casing with outer diameter of 193.7 mm and thickness of 12.7 mm is selected. The elastic modulus of casing material is 2.1×10^5 MPa, and the Poisson's ratio is 0.3. Assuming that the corrosion rate is 0.1 mm/y and the internal pressure is 20 MPa.

3.1. Numerical simulation of casing corrosion

In the framework of ANSYS software, a numerical model of corroded casing is established, in which the influence of stress concentration caused by casing wear on damage evolution is realized by user-defined subroutine.

Numerical model. Owing to symmetry of geometry, load and boundary conditions, the problem is simplified as a two-dimension plane to achieve computational efficiency for a high number of analyses. The finite element model of worn casing is shown in Fig. 4. The internal pressure of p_i is loaded on inner wall of casing. The finite element mesh is divided by planar eight node isoparametric elements and the mesh independence study is conducted. The result of mesh independence study indicates that the maximum mesh size of 0.2 mm can ensure the accuracy of numerical model.

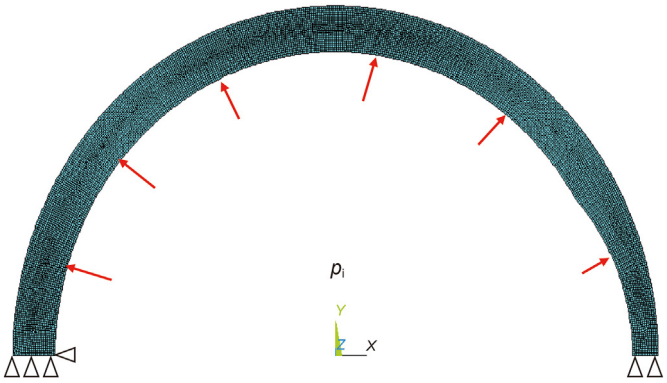

Fig. 4. Finite element model of worn casing.

An example of the corrosion calculation process by numerical simulation is shown in Fig. 5. Firstly, based on the casing parameters and boundary conditions, the geometric model of worn casing is established, and the initial stress at each node is obtained by solving the subroutine. Secondly, the corrosion depth at each node is calculated by Eq. (3), and the new corrosion shape model at the time increment is established. The method of describing the corrosion shape can be expressed by Eqs. (11)–(14). Finally, the burst pressure of corroded casing at the time increment is obtained, and the stress distribution at the next time increment is calculated using the new corrosion shape model.

In polar coordinates, the initial position of each node k on the inner wall can be depicted by

$$k^j = \left(\theta, l_k{}^j\right) \tag{11}$$

where $l_k{}^j$ is the distance from node k to the center of the circle; θ is the angle between node k and the center of the circle.

In a time-element, the corrosion depth at each node can be depicted by

$$\delta^j = \left[\delta_1{}^j \cdots \delta_k{}^j \cdots \delta_N{}^j\right] \tag{12}$$

where N is the total number of nodes on the inner wall of the casing; j is the time element; δ^j is the corrosion depth of the node in a time increment.

After corrosion, the distance from node k to the center of circle is calculated by

$$l_k{}^{j+1} = l_k{}^j + \delta_k{}^j \tag{13}$$

The new polar coordinates of node k

$$k^{j+1} = \left(\theta, l_k{}^{j+1}\right) \tag{14}$$

3.2. Validation of corrosion depth prediction

Corrosion depth is the key to realizing the prediction of casing burst strength, and the accurate prediction of corrosion depth depends on the calculation of hoop stress. In order to solve the confusion problem of stress distribution of damaged casing and improve the prediction accuracy of corrosion depth, numerical simulation is carried out to verify the prediction accuracy of stress distribution for different simplified models.

Taking a casing with an initial wear depth of 40%. By solving the finite element model of the corroded casing, the corrosion morphology of the inner wall of the worn casing under different corrosion time is shown in Fig. 6. With the increase of corrosion time, the remaining wall thickness of the worn casing decreases continuously, especially at the deepest wear position where the wall thickness decreases the most.

The time-variant maximum hoop stress and remaining wall thickness of the corroded casing are shown in Fig. 7. The maximum hoop stress of corroded casing under different corrosion times is shown in Fig. 7(a). The results indicate that the maximum hoop stress calculated by the slot ring model is in good agreement with the numerical model for most of the corrosion time. Specifically, when the corrosion time is eighth year, the maximum relative error

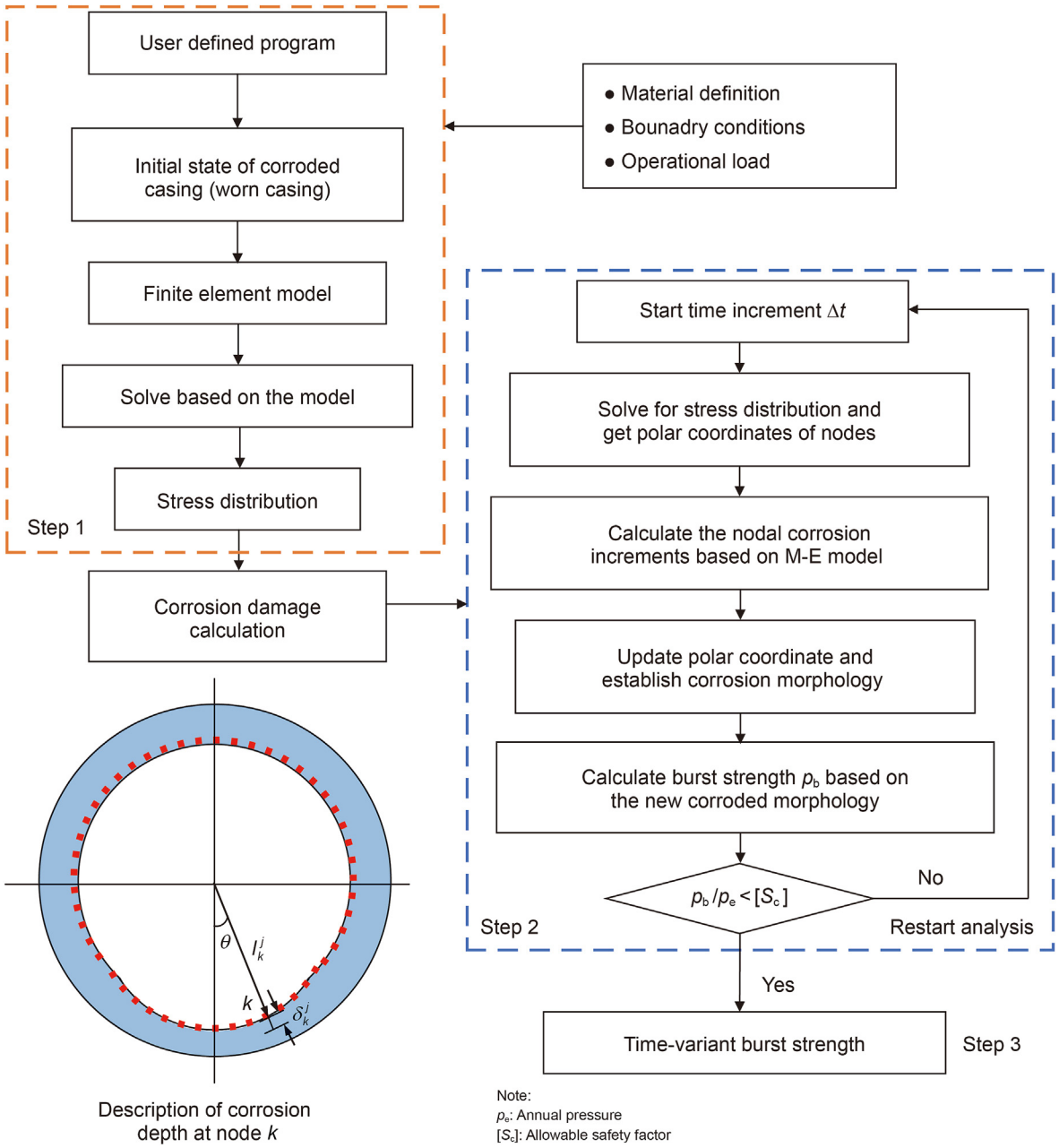

Fig. 5. An example of corrosion calculation process.

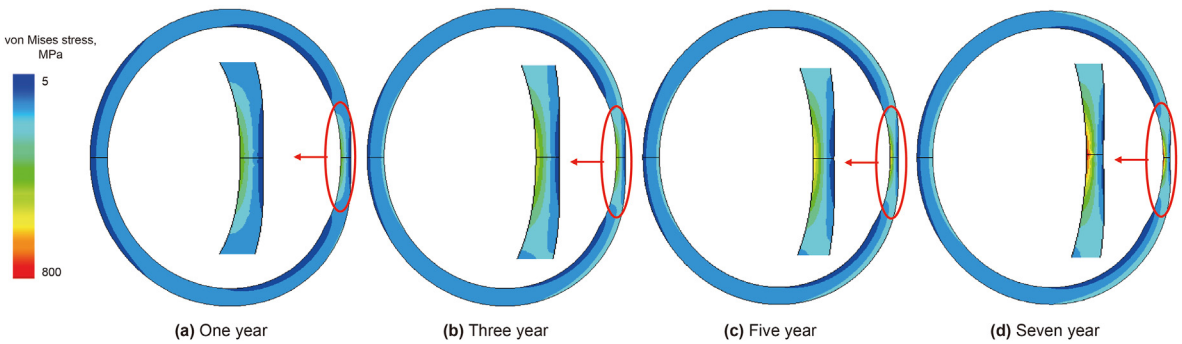

Fig. 6. Corrosion morphology of worn casing under different corrosion time.

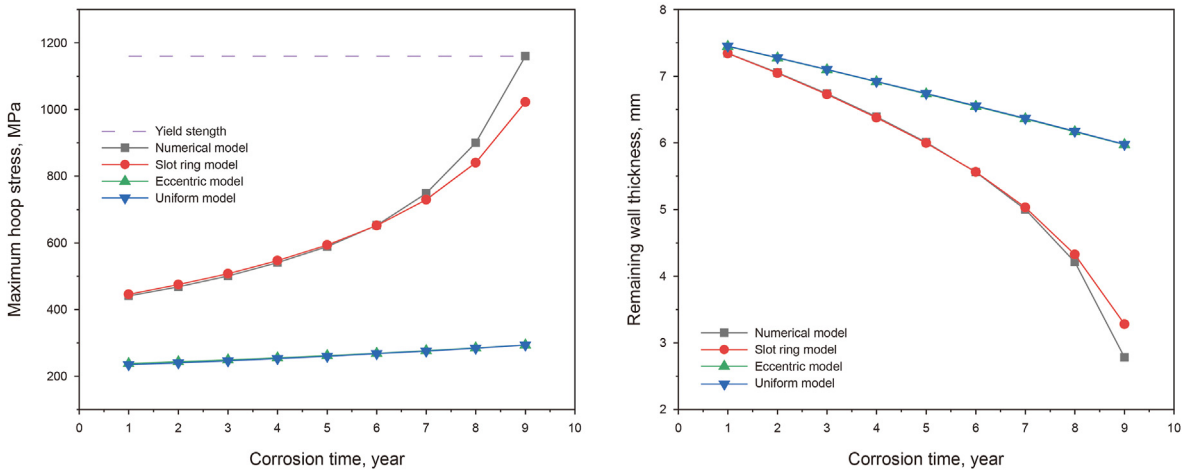

(a) Time-variant maximum hoop stress **(b)** Time-variant remaining wall thickness

Fig. 7. Time-variant maximum hoop stress and remaining wall thickness of corroded casing.

of the maximum hoop stress is 6.7%. The remaining wall thickness of corroded casing under different corrosion time are shown in Fig. 7(b). The results indicate that the remaining wall thickness calculated by the slot ring model is also in good agreement with the numerical model for most of the corrosion time. Specifically, when the corrosion time is eighth year, the maximum relative error of the remaining wall thickness is 2.7%. When the corroded casing is close to the yield state in the ninth year, the relative error between the slot ring model and the numerical model will further increase, indicating that the calculation of the slot ring model in the elastic range is reasonable. Compared with the numerical model, the relative error of the eccentric model and the uniform model increase with the corrosion time. Therefore, the optimal hoop stress prediction model for calculating the corrosion depth is the slot ring model.

3.3. Validation of casing burst strength prediction

In order to evaluate the prediction accuracy of casing burst strength, the prediction results of different theoretical models are compared with the numerical simulation results.

Failure criteria of numerical model. The stress distribution state of the casing and elements in the radial direction at the worn location are shown in Fig. 8, and the calculation of strength is based on the criterion that the von Mises stress in the middle of the remaining wall of the worn location reach the yield strength (Zhang et al., 2022). The results indicate that the significance stress concertation effect occurs at the most severely worn location.

Burst strength of worn casing. When corrosion depth is zero, the models built in this work can also be used to predict the burst pressure of worn casing. To verify the accuracy of the formula developed for the worn casing, comparisons of the results obtained with those obtained from the numerical model, experimental data (Zhang et al., 2022), slot ring model, eccentric model, and uniform model are conducted, as shown in Fig. 9. The result shows that the uniform model provides lower internal pressure capacity than slot ring model and eccentric model. The slot ring model and the eccentric model agree well with the numerical model and experimental data. Specifically, the maximum relative error between the slot ring model and experimental data is 7.4%, the maximum relative error between the eccentric model and experimental data is 7.6%, and the maximum relative error between the numerical model and experimental data is 3.9%. It is demonstrated that the numerical model has the highest prediction accuracy, and the slot

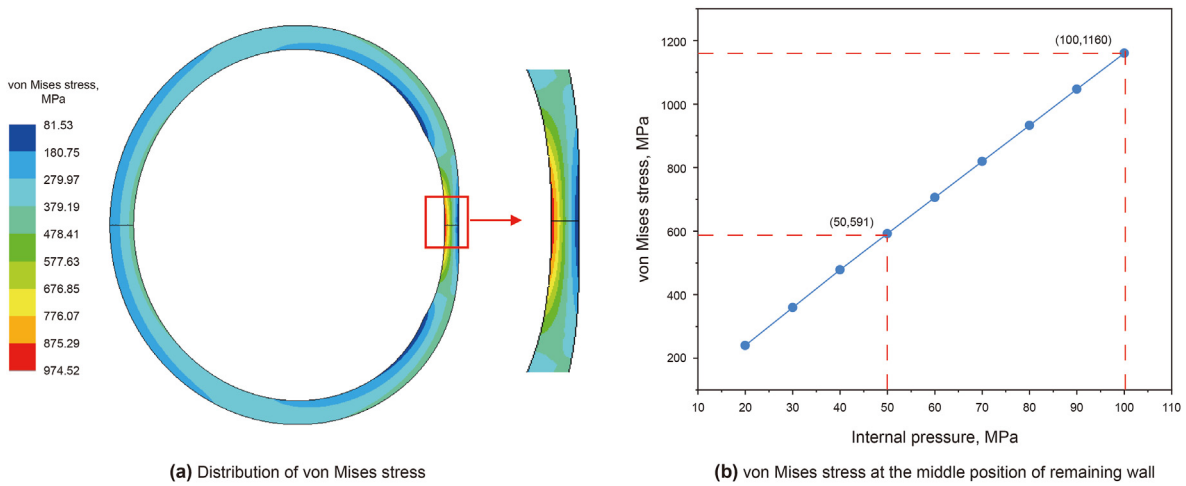

(a) Distribution of von Mises stress **(b)** von Mises stress at the middle position of remaining wall

Fig. 8. The stress state of worn casing.

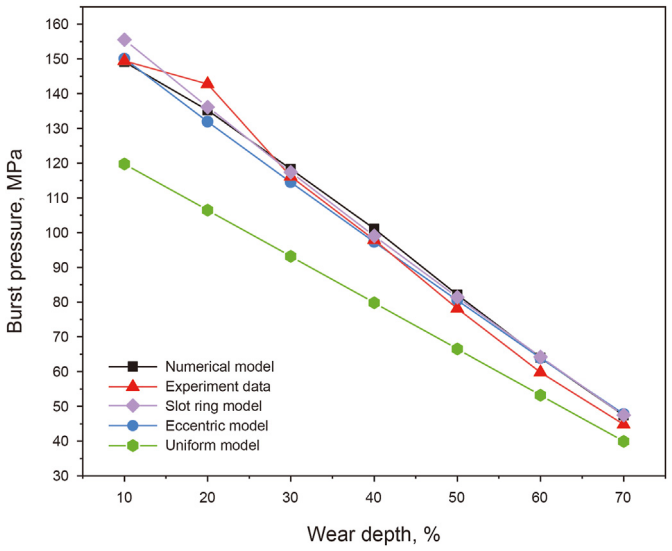

Fig. 9. Comparisons of the results from experimental data, numerical model, and theoretical models.

ring model in the theoretical model is more suitable for predicting the strength of worn casing.

Burst strength of corroded casing. When the corrosion depth is determined, the time-variant burst pressure of the corroded casing can be obtained by using the strength prediction model established in Section 2.3. The prediction results of the three theoretical models and numerical simulations are shown in Fig. 10(a). It can be seen that the slot ring model and the eccentric model agree well with the numerical model, but the uniform model has a larger relative error. Specifically, the maximum relative error between the slot ring model and the numerical model is 6.7%, the maximum relative error between the eccentric model and the numerical model is 4.9%, and the maximum relative error between the uniform model and the numerical model is 21.9%. It is demonstrated that the eccentric model can better predict the burst pressure of corroded casing. Based on the eccentric model, the influence of the M-E interaction on burst pressure of corroded casing is shown in Fig. 10(b). If the M-E interaction is not considered, the corrosion rate will not be accelerated, and the burst pressure of the corroded casing will be overestimated. Compared with the burst pressure considering the M-E interaction, the relative error without considering the M-E interaction in the eighth year is 36.7%.

For the strength of corroded casing, the theoretical model mainly considers the corrosion at the deepest point of wear, and the numerical model considers the corrosion state of the whole inner wall of the worn casing. The results of the eccentric model agree well with the numerical model. It is demonstrated that the main factor affecting the strength degradation of corroded casing is the depth of worn location, and the corrosion in the unworn area has little effect on the strength degradation.

According to the validation of the prediction model of corrosion depth and burst pressure, the most accurate model is determined. For the prediction model of corrosion depth, the slot ring model is the best and is adopted in further calculation; for the prediction model of casing burst pressure, the eccentric model is the best and is adopted in the further calculation.

3.4. Sensitivity analysis of casing strength

Based on the theoretical model, the values of burst pressure and safety factor with time under different initial wear depths and corrosion rates are calculated, and the effects of these factors on burst pressure and safety factor are analyzed.

The safety factor of the corroded casing is calculated by

$$S = \frac{p_b}{p_e} \geq [S_c] \tag{15}$$

where p_e is the casing annulus pressure in MPa; p_b is the burst pressure of corroded casing in MPa; S is the safety factor of corroded casing; $[S_c]$ is the allowable safety factor, which is equal to 1.2.

Initial wear depth. Fig. 11 shows the time-variant burst pressure and safety factor of casing under different initial wear depths when the initial corrosion rate and internal pressure are 0.15 mm/y and 20 MPa, respectively. The results show that with the increase of initial wear depth and corrosion time, the burst pressure and safety factor of casing decreases gradually, and the casing strength decreases rapidly with the corrosion. Compared with service time of the corroded casing with an initial wear depth of 10%, the initial

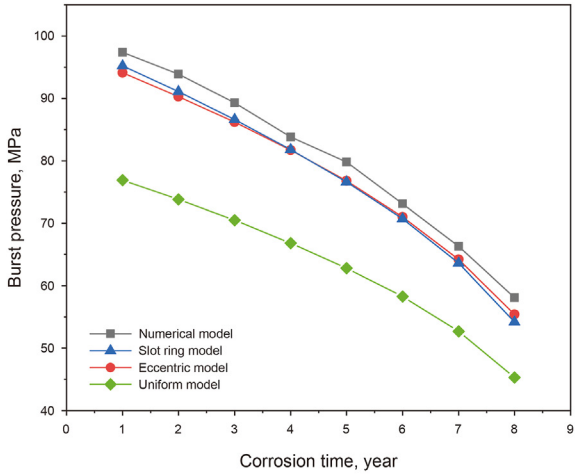

(a) Comparisons of the results from the numerical model and different theoretical models

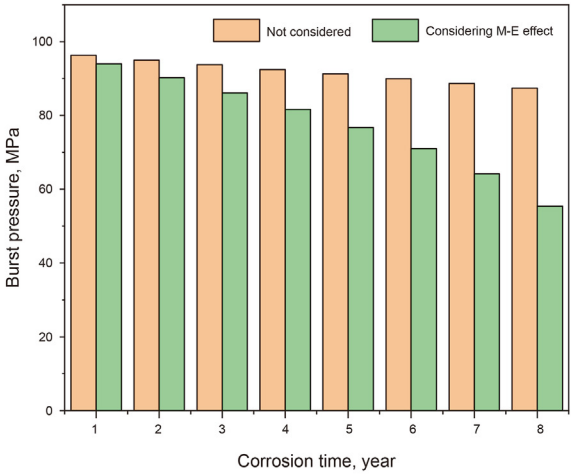

(b) The influence of the M-E effect on burst pressure of corroded casing

Fig. 10. The burst pressure of the corroded casing.

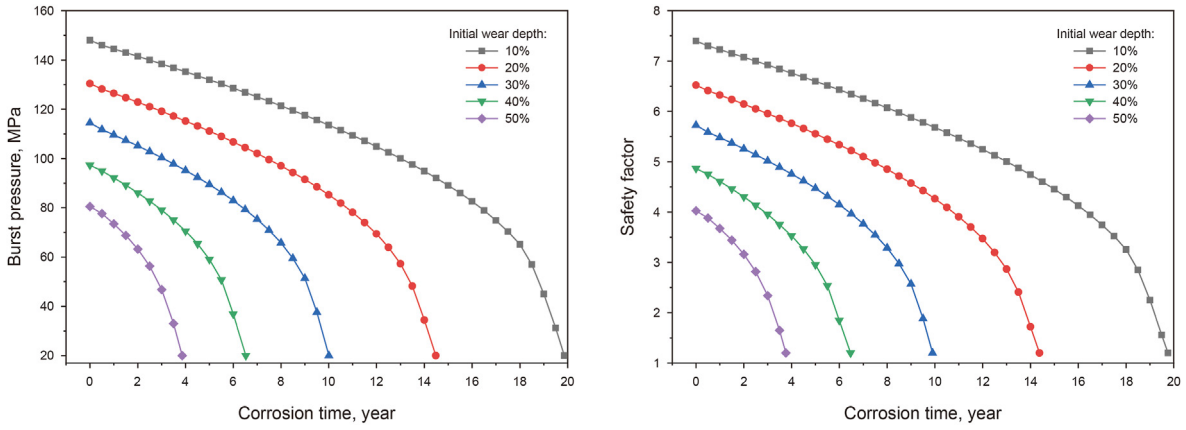

(a) Effect of initial wear depth on burst pressure

(b) Effect of initial wear depth on safety factor

Fig. 11. Effect of initial wear depth on burst pressure and safety factor with time.

wear depth of 50% decreases by about 80%. Therefore, the initial wear depth has a great influence on the burst strength of the corroded casing.

Initial corrosion rate. Fig. 12 shows the time-variant burst pressure and safety factor of casing under different initial corrosion rates when the initial wear depth is 40%. The results show that when the corrosion rate increases from 0.05 to 0.25 mm/y, the safe service time of the casing decreases by 79%. Therefore, the corrosion rate also has a great influence on the burst strength of the corroded casing.

The results indicate that initial wear depth and corrosion rate have a great influence on the burst pressure and service time of corroded casing. Therefore, the initial wear depth and corrosion rate are the main control factors of casing strength.

4. Case study

4.1. Basic data

The severe casing wear occurred in many ultra-deep wells in Northwest China. Take an ultra-deep well X as an example, of which the total well depth is 8270 m, and the setting position of the mechanical packer is 6870 m. The specific well structure is shown in Fig. 13, and the upper annulus at the packer is defined as A, and the lower annulus is defined as B. The production parameters are shown in Table 1.

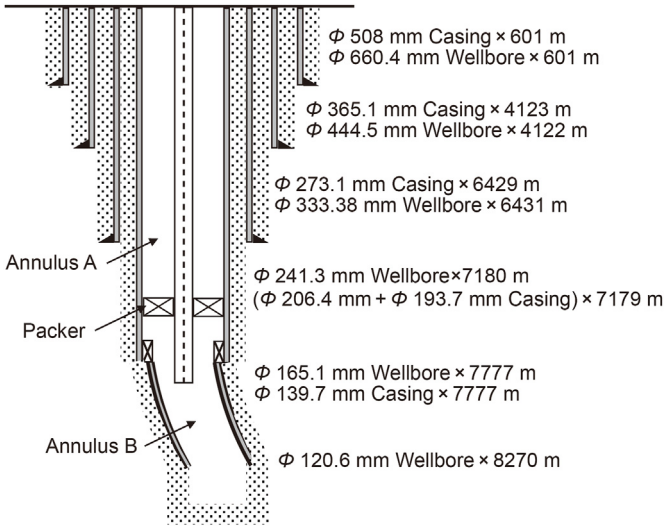

Fig. 13. The well structure.

The casing wear occurred in the whole casing section, in which

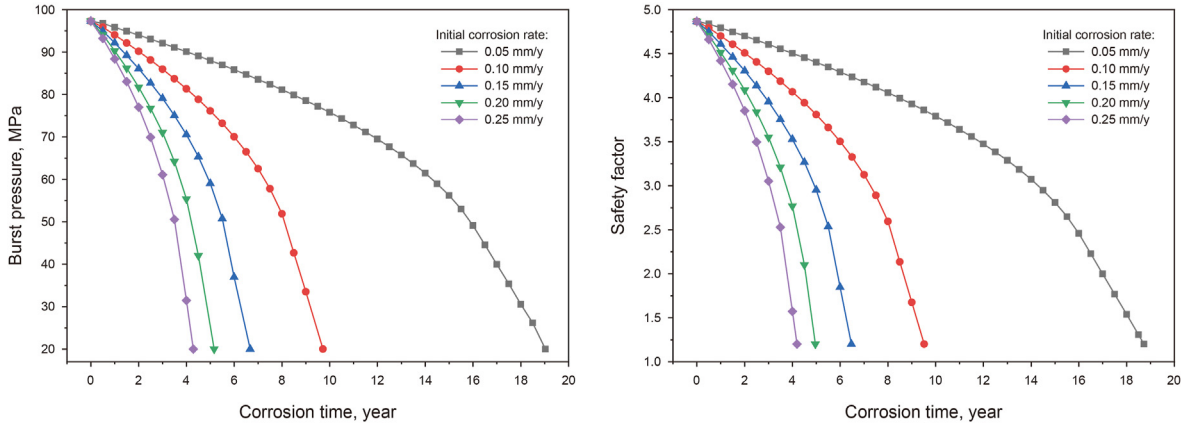

(a) Effect of corrosion rate on burst pressure

(b) Effect of corrosion rate on safety factor

Fig. 12. Effect of initial corrosion rate on burst pressure and safety factor with time.

Table 1
The production parameters of the well.

Parameters	Values	Parameters	Values
Geothermal gradient, °C/m	2.27	Bottom hole temperature, °C	180
Bottom hole pressure, MPa	113	Gas production rate, m^3/d	40×10^4
Oil production rate, m^3/d	140	Water production rate, m^3/d	30
Fluid density in annulus, g/m^3	1.35	Relative density of natural gas, g/m^3	0.597
Friction factor	0.22	Radiative heat transfer coefficient in annulus, W/m·°C	34.28
Thermal conductivity of cement sheath, W/m·°C	0.62	Thermal conductivity of formation, W/m·°C	2.122
Thermal diffusivity of formation, m^2/s	1.21×10^{-6}	Convective heat transfer coefficient in annulus, W/m·°C	1.96

the residual strengths of Φ206.4 mm casing, Φ193.7 mm casing and Φ139.7 mm casing are studied in the corrosive environment. Note that, the strength degradation of production tubing is not studied, because the failed tubing can be easily replaced with another one.

4.2. CO_2 corrosion rate

Temperature and pressure distribution. Temperature and pressure are two important parameters for predicting corrosion rate. According to the distribution model of temperature and pressure established in Appendix C, the temperature and pressure along the wellbore depth direction are calculated by iterative method, and the influence of different production rates on temperature and pressure distribution is analyzed.

Fig. 14 shows the influence of different production rates on temperature and pressure distribution. The results indicate that the temperature distribution changes nonlinearly with well depth, and increases with the increase of production rate. The distribution of pressure mainly depends on the density of the annulus liquid, so the production rate has little effect on it.

Effect of partial pressure and production rate. The prediction model of CO_2 corrosion rate is shown in Appendix C. By introducing the pressure-temperature varying law into the prediction model of CO_2 corrosion rate, the initial corrosion rate of the casing string is obtained, and the influences of CO_2 partial pressure and gas production on corrosion rate are analyzed. Fig. 15(a) shows the influence of different partial pressures on corrosion rate when the production rate is 40×10^4 m^3/d. Fig. 15(b) shows the influence of different production rates on corrosion rate when the partial pressure is 3 MPa.

The results show that the corrosion rate of casing increases first and decreases subsequently with the increase of well depth. Increasing the partial pressure of CO_2 can lead to the occurrence position of maximum corrosion rate of casing moving towards the wellhead and an increase in the corrosion rate. Increasing the production rate can lead to the occurrence position of the maximum corrosion rate of casing moving towards wellhead, but it has no effect on the maximum corrosion rate. When the gas production rate is 60×10^4 m^3/d, the wellhead temperature exceeds the critical temperature of the corrosion product film, resulting in the maximum corrosion rate at the wellhead.

4.3. Burst strength of corroded casing

Based on the operation of the well, the average production rate is 40×10^4 m^3/d, and the average partial pressure is 3 MPa. The time-variant remaining wall, burst pressure, and safety factor of the casing string is calculated by the theoretical model. Fig. 16 shows the distribution of the maximum wear depth and the variation of the remaining wall of worn casing under different corrosion time. The maximum wear depth of casing is measured with a caliper instrument, and the results show severe casing wear throughout the entire well section; meanwhile, the maximum wear depth overall decreases with the increase of well depth. With the increase of corrosion time, the remaining wall of the worn casing in the deep section is rapidly reduced. Besides, the casing section below the

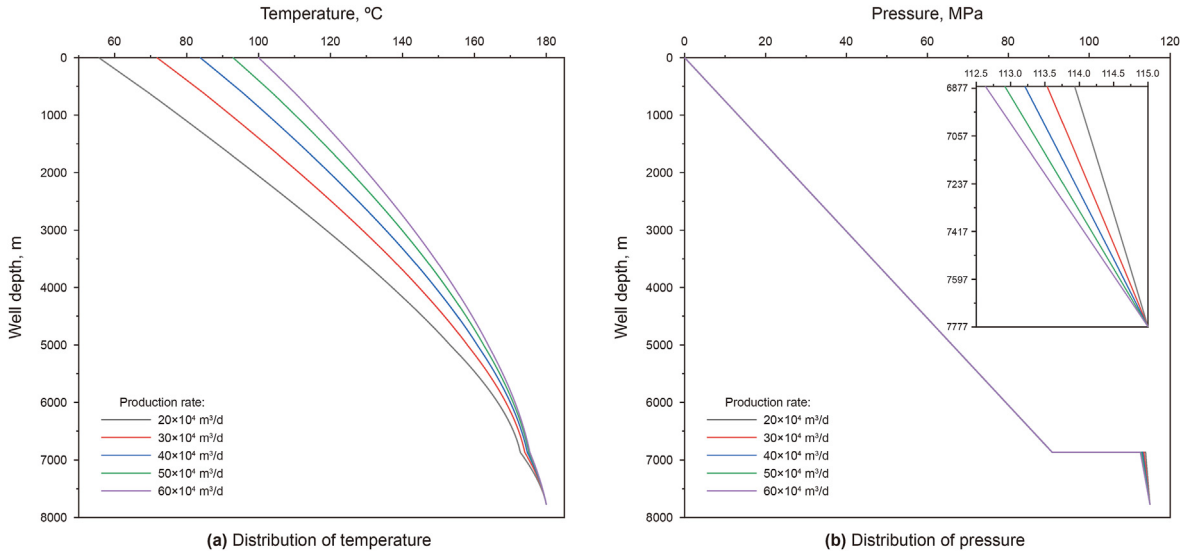

Fig. 14. Effect of production rate on distribution of temperature and pressure.

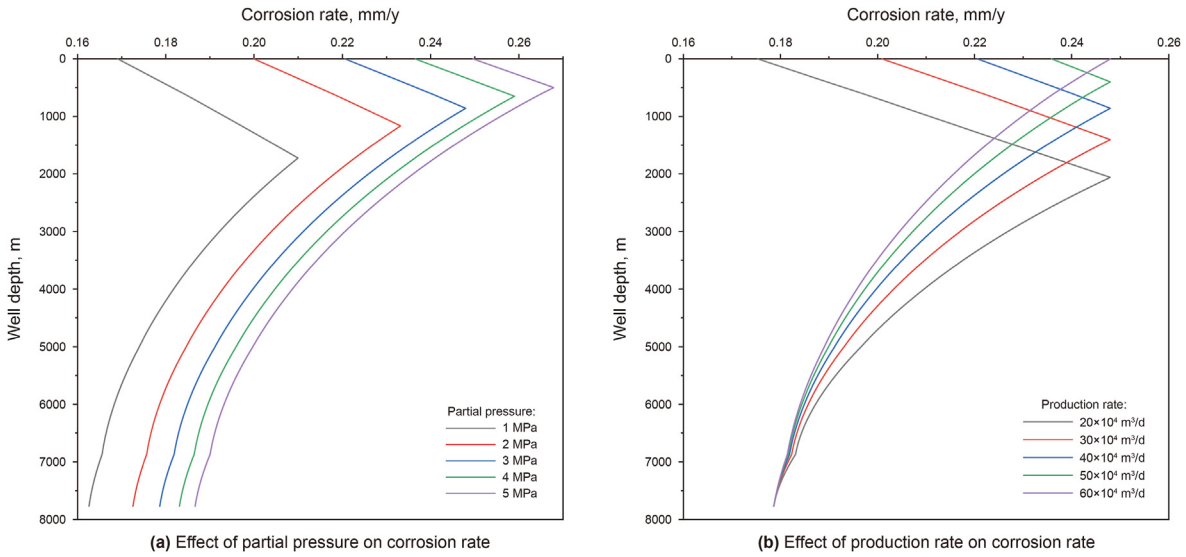

Fig. 15. Effect of partial pressure and production rate on corrosion rate.

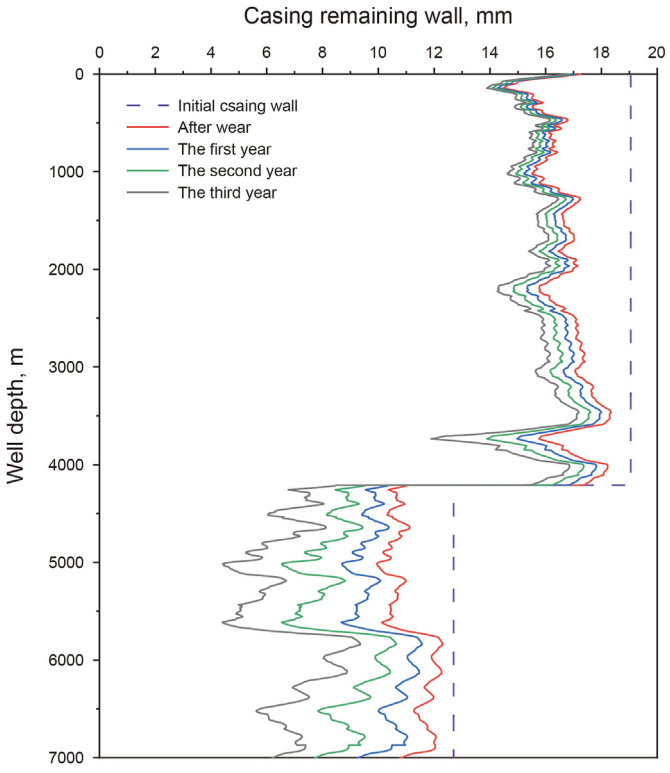

Fig. 16. The remaining wall of worn casing under different corrosion time.

mechanical packer is not shown in the results.

The burst pressure and safety factor of the worn casing under different corrosion time are shown in Fig. 17, and the strength of unworn casing is given by the casing manufacturer. Fig. 17(a) depicts the variation of casing burst pressure. When the corrosion time reaches the third year, some casing sections are severely damaged because the burst pressure is close to the annulus pressure. Therefore, the strength degradation of worn casing is very serious under high temperature, high pressure, and corrosive environment. Fig. 17(b) shows the result of the time-variant safety factor of worn casing. The well sections of 4867–5712 and 6400–6870 m have reached the allowable safety factor under the third year, as shown in the red arrows. Therefore, there is a severe risk of failure in some downhole sections.

The field application shows that many wells in this oilfield have serious failure problems with casing integrity after 2–3 years of production, and the corrosion of worn casing is regarded as the important reason. The prediction of casing service time shows that our results are close to field application, so the models built in this paper can provide effective guidelines for the assessment of casing integrity.

4.4. Service time of corroded casing

At present, there have been many technical measures to reduce the negative impact of casing wear and corrosion. The measures to reduce wear mainly include using casing of larger wall thickness, decreasing dogleg severity in the drilling process, installing wear reduction connectors on drill strings and so on. The measures to reduce corrosion mainly include adding corrosion inhibitors, using the technology of cathodic protection and optimizing corrosion-resistant steel casing, etc.

In the well section with severe strength degradation, the initial wear depth is less than 2.5 mm, and the corrosion rate is less than 0.25 mm/y. In order to analyze the effect of protective measures on the service time of casing, the values of service time under different initial wear depths and corrosion rates are calculated. Take a casing with an annulus pressure of 70 MPa and a temperature of 160 °C as an example. The service time of casing under different initial wear depths and corrosion rates are shown in Fig. 18. When the initial wear depth decreases from 2.5 to 0.5 mm, and the initial corrosion rate decreases from 0.25 to 0.05 mm/y, the service time of corroded casing increases by about ten times. If the initial wear depth and corrosion rate are controlled within 1.5 mm and 0.15 mm/y, the service life of the wellbore can be improved to more than eight years.

For a specific well, the casing safety service life chart can be established according to the well structure and production parameters, and the reasonable wear depth and corrosion rate of the casing can be predicted, which has important guiding significance to improving the casing integrity of deep and ultra-deep wells, ensuring the safety of the wellbore, and extending the service time

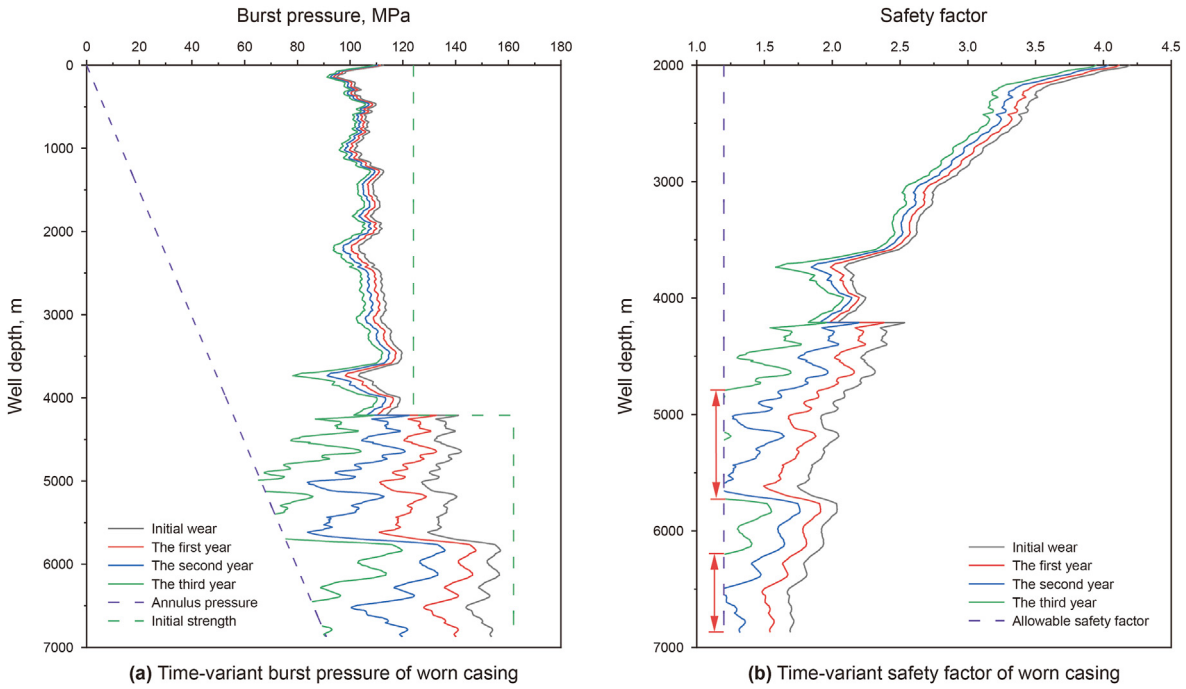

Fig. 17. The burst pressure and safety factor of the worn casing under different corrosion time.

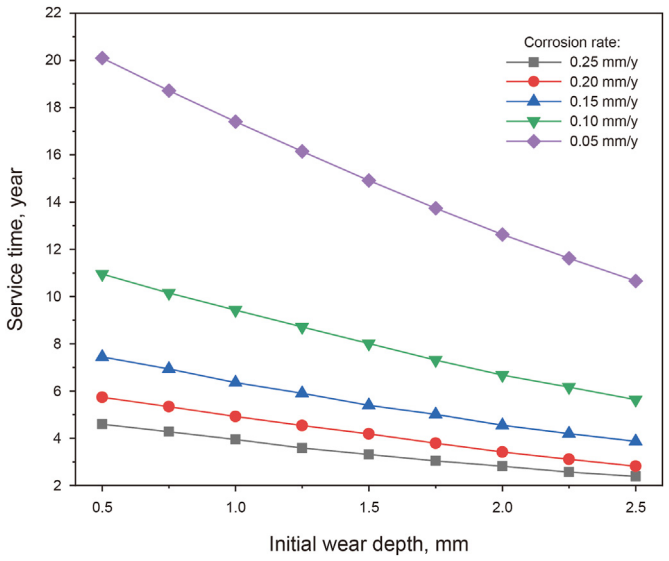

Fig. 18. Service time of corroded casing at different initial wear depths and corrosion rates.

of the wellbore.

5. Conclusions

1. Casing wear defects cause stress concentration and enhance the M-E interaction, resulting in a rapid increase in corrosion depth and a significant decrease in casing strength.
2. The burst pressure of the corroded casing will be overestimated if the M-E interaction is neglected. The burst pressure without considering the M-E interaction is over one-third higher than the result of considering the M-E interaction at the later corrosion stage.
3. The verification with numerical simulation indicates that the slot ring model is the most accurate for predicting the corrosion depth, and the eccentric model is the most accurate for predicting the burst pressure of corroded casing.
4. The critical influence factors on the casing service life are the casing wear depth and corrosion rate. When the wear depth is at a certain value, the reduction in the corrosion rate by 80% can increase the casing service life by about five times. Therefore, the coupling effect between wear and corrosion should be sufficiently considered in casing integrity evaluation and production design.
5. The casing strength of gas well containing CO_2 is evaluated, but the casing thinning due to CO_2–H_2S is not considered in this paper. The existence of H_2S also affects the corrosion process of casing, and even causes more complex corrosion cracking in some oilfields. Therefore, the influence of acid gas coexistence on casing strength needs further study.

Declaration of interests

The authors declare that they have no known competing financial interests or personal relationships that could have appeared to influence the work reported in this paper.

Acknowledgments

The authors gratefully acknowledge the financial support from the Natural Science Foundation of China (Grant numbers: 52222401, 52234002, 51904317, 51821092) and Science Foundation of China University of Petroleum-Beijing (Grant number: ZX20230083).

Appendix A. Mechano-electrochemical effect of casing corrosion system

According to the thermodynamics theory, the relationship

between the chemical potential and its activity is expressed as

$$\mu = \mu_o + RT\ln a \tag{A-1}$$

where μ is the chemical potential in V; μ_o is the standard state chemical potential in J/mol; a is the thermodynamic activity in dimensionless.

In addition, the electrochemical potential $\overline{\mu}$ is expressed as

$$\overline{\mu} = \mu_o + RT\ln a + zF\varphi = \mu_o + RT\ln\overline{a} \tag{A-2}$$

where z is the valence of metal ions; F is the Faraday constant in C/mol.

For metal, the relationship between chemical potential and pressure can be expressed as:

$$\Delta\mu = \int_{P_1}^{P_2} V(P)\mathrm{d}P = \int_{P_1}^{P_2} V_o \exp(-\chi P)\mathrm{d}P \approx V_o\Delta P \tag{A-3}$$

$$\varphi = \frac{RT}{zF}\ln\left(\frac{a^0}{a_0}\right) - \frac{\Delta PV}{zF} \tag{A-7}$$

where φ is the equilibrium potential in V; a_0 is the standard activity, dimensionless; a^0 is the thermodynamic activity under the equilibrium condition.

As can be seen from Eq. (A-7), the equilibrium potential of the cation system is decreased due to the mechanical effect, and its reduction value can be set as $\Delta\varphi = \Delta PV/zF$.

Appendix B. Prediction model of hoop stress

Theoretical analysis of slot ring model. The slot ring model, as shown in Fig. B-1, simplifies the damaged shape as a slot ring, where the circle with radius r_i and center o_1 represents the nominal inner wall of the casing. The wear depth is w, and the corrosion depth is $\delta(t)$.

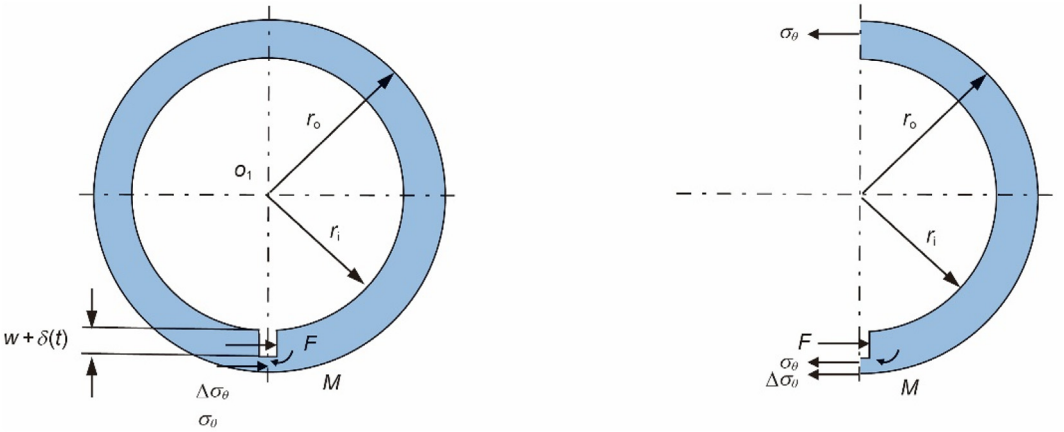

Fig. B-1. Coupling model of wear and corrosion for slot ring model

where V_o is the metal molar volume before deformation in m^3/mol; ΔP is the residual pressure in MPa; χ is the compressibility coefficient of metal, equal approximately to 10^{-6}.

When the metal is loaded with pressure, the chemical potential is expressed as

$$\tilde{\mu} = \mu_{\Delta P=0} + \Delta PV = \mu_0 + RT\ln a + \Delta PV = \mu_0 + RT\ln\tilde{a} \tag{A-4}$$

where $\tilde{a}$ is the mechanical-chemical activity, equal to $a\exp(\Delta PV/RT)$.

For casing corrosion system, the casing is subjected to pressure in acidic solution, and there are both mechanical conditions and electrochemical factors. The mechano-electrochemical potential can be expressed as

$$\tilde{\overline{\mu}} = \mu_0 + RT\ln a + \Delta PV + zF\varphi = \mu_0 + RT\ln\tilde{\overline{a}} \tag{A-5}$$

The mechanical-electrochemical activity $\tilde{\overline{a}}$ is

$$\tilde{\overline{a}} = a\exp\left(\frac{zF\varphi + V\Delta P}{RT}\right) \tag{A-6}$$

When the corrosion reaction reaches equilibrium in any corrosion system ($\tilde{\overline{\mu}}\to 0$), assuming the $\mu_0 = -RT\ln a_0$, the equilibrium potential of the corrosion system is obtained.

When casing is integrated, the hoop stress can be expressed by the Lame equation

$$\sigma_\theta = \frac{p_i r_i^2 - p_o r_o^2}{r_o^2 - r_i^2} + \frac{(p_i - p_o)r_i^2 r_o^2}{r_o^2 - r_i^2}\frac{1}{r^2} \tag{B-1}$$

Comparing with a casing without wear and corrosion, the loss of hoop stress plus the exposure of internal pressure on the damaged wall portion of a damaged casing is equal to a hoop force F

$$F = \int_{r_i}^{r_i+w+\delta(t)} (p_i + \sigma_\theta)\mathrm{d}r \tag{B-2}$$

$$F = p_i(w+\delta(t)) + \frac{p_i r_i^2}{r_o^2 - r_i^2}(w+\delta(t)) + \frac{p_i r_i^2 r_o^2}{r_o^2 - r_i^2}\frac{(w+\delta(t))}{r_i(r_i + w + \delta(t))} \tag{B-3}$$

The casing hoop stress increase ($\Delta\sigma_\theta$) in the remaining wall of damaged casing is expressed as

$$\Delta\sigma_\theta = \frac{F}{(t - w - \delta(t))} \tag{B-4}$$

To maintain a force-moment balance, the bending moment in

the remaining wall of damaged casing is induced. With ignoring casing deformation, this bending moment is expressed as

$$M=\Delta\sigma_\theta(t-w-\delta(t))\left(r_o-\frac{t-w-\delta(t)}{2}\right)-F\left(r_i+\frac{w+\delta(t)}{2}\right) \tag{B-5}$$

The bending hoop stress caused by the bending moment is expressed as

$$\Delta\sigma_{\theta,m}=\frac{M\left(r-\frac{r_i+w+\delta(t)+r_o}{2}\right)}{I}=\frac{3Ft(2r-r_i-r_o-w)}{(t-w-\delta(t))^3} \tag{B-6}$$

Considering the above the influencing factors, the hoop stress of damaged is expressed as

$$\sigma_{\theta,t}=\frac{p_i{r_i}^2}{{r_o}^2-{r_i}^2}+\frac{p_i{r_i}^2{r_o}^2}{{r_o}^2-{r_i}^2}\frac{1}{r^2}+\frac{F}{t_o-w-\delta(t)}-\frac{1.95F(2r-r_o-r_i-w-\delta(t))}{(t_o-w-\delta(t))^2} \tag{B-7}$$

Theoretical analysis of eccentric model. The damaged casing is approximately taken as casing with geometric eccentricity. The eccentric model is shown in Fig. B-2, where the circle with radius r_2 and center o_2 represents the nominal inner wall of the eccentric pipe. The theoretical outer radius and the center of the undamaged casing are r_1 and o_1. The wear depth is w, and the corrosion depth is $\delta(t)$.

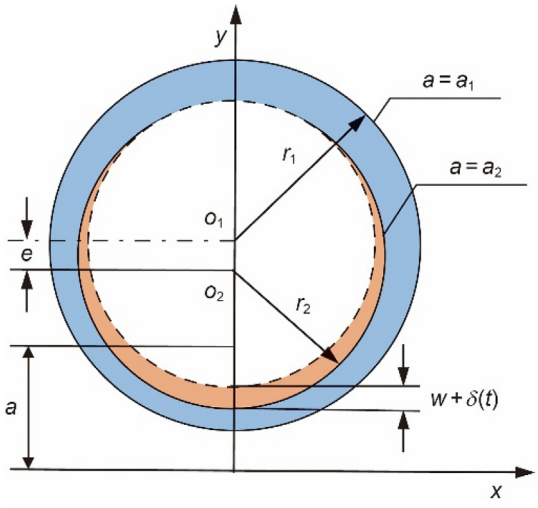

Fig. B-2. Coupling model of wear and corrosion for eccentric model

Eccentric wear model involves two eccentric circular boundaries which can be better expressed in bipolar coordinate system. The relationship between the bipolar coordinate (α, β) and the cartesian coordinates (x, y) can be expressed as follows

$$z=x+\mathrm{i}y=\mathrm{i}a\coth\frac{\zeta}{2},\zeta=\alpha+\mathrm{i}\beta \tag{B-8}$$

where:

$$x=\frac{a\sin\beta}{\cosh\alpha-\cos\beta},y=\mathrm{i}\frac{a\sinh\alpha}{\cosh\alpha-\cos\beta} \tag{B-9}$$

where ζ is the complex variable about the bipolar coordinates (α, β); z is the complex variable about the Cartesian coordinates (x, y) and $\mathrm{i}=\sqrt{-1}$; a is a real constant.

Eliminating β from Eq. (B-9) yields

$$x^2+(y-a\coth\alpha)^2=(a\,\mathrm{csch}\,\alpha)^2 \tag{B-10}$$

Eq. (B-10) represents a circle with radius cschα and center (0, cothα). Therefore, the inner boundary or outer boundary can be described by given $\alpha=\alpha_1$ or $\alpha=\alpha_2$.

The outer boundary radius r_1, inner boundary radius r_2, eccentric distance e and constant a are expressed as

$$r_1=\frac{a}{\sinh\alpha_1},r_2=\frac{a}{\sinh\alpha_2} \tag{B-11}$$

$$a=\frac{\sqrt{{r_1}^4+{r_2}^4-{r_1}^2{r_2}^2-2e^2{r_2}^4-2e^2{r_1}^2+e^4}}{2e} \tag{B-12}$$

$$e=a(\coth\alpha_2-\coth\alpha_1) \tag{B-13}$$

The stress distribution of eccentric pipe can be obtained by complex potential theory (Timoshenko and Goordier, 1972)

$$a(\sigma_\alpha+\sigma_\beta)=2B[2\sinh\alpha\cosh\beta-\sinh 2\alpha\cosh 2\beta]-2C[1-2\cosh\beta\cos\beta+\cosh 2\beta\cos 2\beta]+4eA \tag{B-14}$$

$$\begin{aligned}a(\sigma_\beta-\sigma_\alpha+2\mathrm{i}\tau_{\alpha\beta})=&-2B[(\sinh 2\alpha-2\sinh 2\alpha\cos\alpha\cos\beta\\&+\sinh 2\alpha\cos 2\beta)\\&-\mathrm{i}(2\cosh 2\beta)\cosh\alpha\sin\beta-\cosh 2\alpha\sin 2\beta]\\&+2C[-\cosh 2\alpha+2\cosh 2\alpha\cosh\alpha\cos\beta-\cosh 2\alpha\cos 2\beta\\&+\mathrm{i}(2\sinh 2\alpha\cos\alpha\sin\beta-\sinh 2\alpha\sin 2\beta)]\\&+D[\sinh 2\alpha-2\sinh\alpha\cosh\beta-\mathrm{i}(2\cosh\alpha\sin\beta-\sin 2\beta)]\end{aligned} \tag{B-15}$$

where σ_α is the radial stress of eccentric pipe; σ_β is the hoop stress of eccentric pipe; $\tau_{\alpha\beta}$ is the shear stress of eccentric pipe, A, B, C and D are the integral constants to be determined by the stress boundary conditions.

Under internal pressure p_i, the stress boundary conditions can be determined by

$$\begin{cases}(\sigma_\alpha)_{\alpha=\alpha_1}=-p_i,(\tau_{\alpha\beta})_{\alpha=\alpha_1}=0\\(\sigma_\alpha)_{\alpha=\alpha_2}=0,(\tau_{\alpha\beta})_{\alpha=\alpha_2}=0\end{cases} \tag{B-16}$$

Simultaneously solving Eqs. (B-14)–(B-16) yields the following relationships:

$$\begin{cases}2B=D\dfrac{\cosh(\alpha_1+\alpha_2)}{\cosh(\alpha_1-\alpha_2)}\\2C=-D\dfrac{\sinh(\alpha_1+\alpha_2)}{\cosh(\alpha_1-\alpha_2)}\\A=-\dfrac{1}{2}\dfrac{p_i\sinh^2\alpha_2}{\sinh^2\alpha_1+\sinh^2\alpha_2}\\D=-a\dfrac{-p_i\coth(\alpha_1-\alpha_2)}{\sinh^2\alpha_1+\sinh^2\alpha_0}\end{cases} \tag{B-17}$$

Substituting A, B, C and D in Eq. (B-17) into those in Eqs. (B-14) and (B-15), the hoop stress distribution of inner boundary of eccentric model is expressed as

$$(\sigma_\beta)_{\alpha=\alpha_1}=\frac{p_i}{m}\left[\frac{-2\cos\beta\sinh\alpha_2+\sinh(\alpha_1+\alpha_2)}{\sinh(\alpha_1-\alpha_2)}-\cos2\beta-2\sinh^2\alpha_2\right]+p_i \tag{B-18}$$

where $m = \sinh^2\alpha_1 + \sinh^2\alpha_2$.

Theoretical analysis of uniform model. To facilitate theoretical analysis, the crescent-shaped worn casing is approximately taken as casing with geometric.

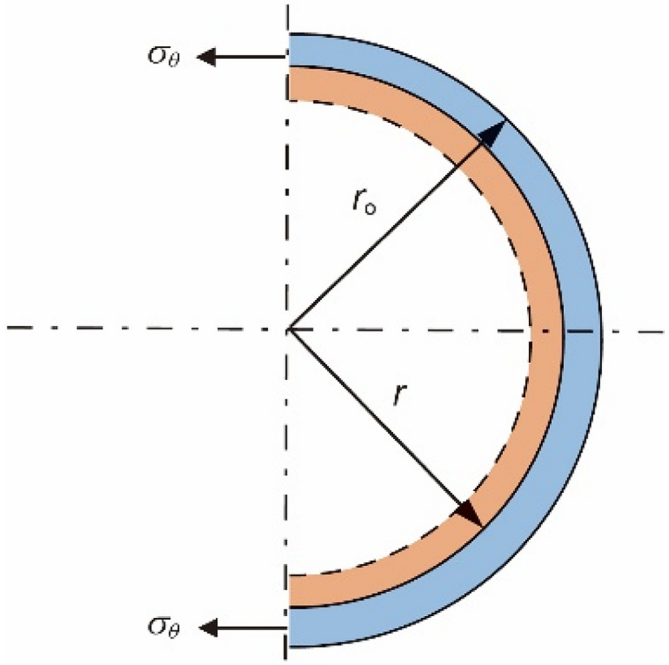

Fig. B-3. Coupling model of wear and corrosion for uniform model

When a uniform thickness reduction around the casing inner wall, the hoop stress is always balancing with the casing internal pressure. The balance equation of force is expressed as

$$2\sigma_\theta h=\int_0^\pi p_i\sin\theta r d\theta \tag{B-19}$$

where h is the remaining wall of the casing, $r = r_i + w + \delta(t)$.

By solving the balance equation, the hoop stress is expressed as

$$\sigma_\theta=\frac{p_i r}{h} \tag{B-20}$$

Appendix C. Prediction model of CO_2 corrosion rate

One of the keys to corrosion problem is the prediction of corrosion rate. Corrosion is mainly affected by factors such as CO_2 partial pressure, H_2S partial pressure, temperature, pressure and pH value. At present, there are mainly three models (Zhang et al., 2020) of corrosion rate prediction: empirical model, semi-empirical model and mechanism model. Since different prediction models have different applicable conditions, it is necessary to choose a reasonable prediction model in accordance with the production characteristics of the well.

In this paper, according to the characteristics that the gas well is mainly affected by CO_2 corrosion, the de Waard model (De Waard et al., 1991) is selected to predict the corrosion rate. As a semi-empirical model, the theoretical model is first established, and then the weight of each influencing factor is determined through experiments, so a small amount of experimental data can meet the requirements (Li and Liu, 2020). It is assumed that corrosion in CO_2 containing environments is controlled by activation reaction where the concentration of the reacting species is dependent upon the partial pressure of CO_2. The system constants, e.g., activation energy, Henry's Law constant, reaction order etc., for the model are then gathered together and the resulting equation and unified constants fitted to a series of laboratory test results. The equation for corrosion prediction of CO_2 is shown as

$$\log(V_o)=5.8-\frac{1710}{(T+273.15)}+0.67\log(p_{co_2}) \tag{C-1}$$

where T is the temperature in °C; p_{CO_2} is the CO_2 partial pressure in MPa; V_o is the corrosion rate in mm/y.

For the prediction model, the influences of temperature and partial pressure of CO_2 are mainly considered, and the impact of protective film of $FeCO_3$ on corrosion rate is also included. According to the de Waard model, the equation can be modified by using the results data of corrosion experiment and method of multiple regression. The regression equation is rewritten as

$$\log(V_o)=A+\frac{B}{T}+C\log(p_{co_2}) \tag{C-2}$$

where A, B and C is the undetermined coefficients.

Experiment result data. For purpose of investigating the influence of CO_2 and temperature on corrosion rate, a TP140V casing is used in laboratory to test corrosion rate. The corrosion experiment is divided into three main steps: the first step is samples preparation, including simulating the working environment of casing string and preparing specimens, specimens are 50 × 10 × 3 mm. The second step is test procedure, multiple groups of slices are hanged in the HTHP reactor, deoxygenated with pure nitrogen for 2 h, then adjusting temperature and pressure to planned values. Experiment period is 72 h, the temperature is from 60 to 180 °C with an interval of 30 °C, and partial pressure of CO_2 is from 1 to 5 MPa with an interval of 1 MPa. The final step is post-test processing. After the process of reaction, take out the samples, clear the corrosion product film of sample surface and weigh the sample that is corroded. Then corrosion rate V_o is obtained from

$$V_o=\frac{\Delta w}{\rho A T_t} \tag{C-3}$$

where Δw is the weight loss in g; ρ is the material density in $g\cdot mm^{-3}$; A is the total surface area in mm^2; T_t is the experimental period in hour.

The purpose of this experiment is to obtain the corrosion rate of different temperatures and different partial pressures. Take constant partial pressure 3 MPa and temperature 120 °C as an example. The partial data results of corrosion test are shown in Fig. C-1. With the increase of temperature, the corrosion rate reaches the maximum value, and then decreases. Specifically, under different constant partial pressures, the corrosion rate decreases after the maximum value in the temperature range of 90–120 °C. The corrosion rate increases with the increase of partial pressure.

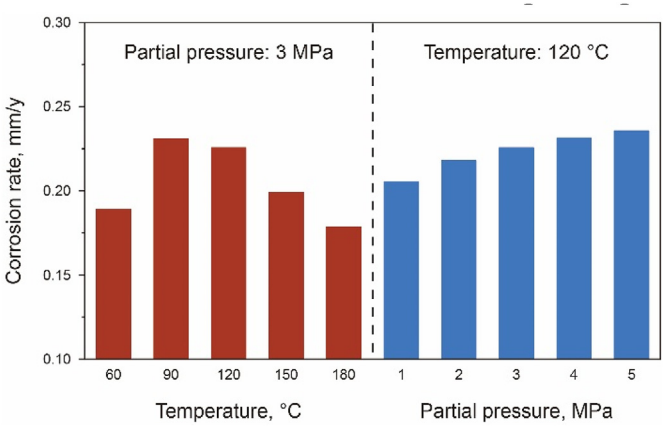

Fig. C-1. The results of corrosion rate test

In the process of post-test, the microstructure of the slices indicate that the corrosion product film controls the corrosion rate, and the smaller the diameter of corroded grain, the stronger the protection effect on surface of slice. Therefore, the reason for the decrease in corrosion rate is obtained. The critical temperature of maximum corrosion rate under different partial pressures are given in Table C-1.

Prediction model of CO_2 corrosion. According to the results of experimental data, a multiple regression is performed based on the de Waard model. The prediction model of corrosion rate is expressed as

$$\log(V_o) = 0.3441 - \frac{955.77}{T} + 0.2421\log(p_{co_2}) \tag{C-4}$$

Considering the influence of corrosion product film on the corrosion rate, the factor of corrosion product film F_{scale} is introduced. This is included as the scale temperature, T_{scale}, as

$$T_{scale} = \frac{2290}{5.9 + 0.5\log p_{co_2}} \tag{C-5}$$

where T_{scale} is the temperature where the corrosion rate goes through a maximum.

When the temperature exceeds the scale temperature, the F_{scale} is used to correct the corrosion rate V_o given by

$$\log(F_{scale}) = \begin{cases} T > T_{scale}, 1649\left(\dfrac{1}{T} - \dfrac{1}{T_{scale}}\right) \\ T \le T_{scale}, 0 \end{cases} \tag{C-6}$$

Table C-1
The critical temperature of maximum corrosion rate under different partial pressures

Partial pressure, MPa	1	2	3	4	5
Temperature, °C	115.1	105.5	100.1	96.3	93.4

The results of multiple regression indicate that the expression accurately captures the results from experimental data with an R^2 values of 0.9967, 0.9987 and 0.9942, respectively.

Temperature and pressure distribution. By introducing the pressure-temperature law into the prediction model of CO_2 corrosion rate, the corrosion rate of the casing string in CO_2 corrosion environment can be obtained. In the test of wellbore temperature and pressure, the high temperature and high pressure have strict requirements on test equipment. Only the temperature and pressure at the bottom of the well or wellhead can be measured, and then the theoretical model is used to predict the distribution of wellbore temperature and pressure. Based on the momentum conservation, energy conservation and non-ideal gas state equations, the coupled prediction model of temperature and pressure distribution is developed (Hasan et al., 1998; Shi et al., 2018), and its expression is shown as

$$\begin{cases} \dfrac{dp}{dx} = \left[-\rho g\sin\theta - f\dfrac{\rho v^2}{2d}\right] \Big/ \left(1 - \dfrac{\rho v^2}{p}\right) \\ \dfrac{dT}{dx} = \left\{\dfrac{2\pi r_{to}U_{to}k_e}{w[r_{to}U_{to}f(t)+k_e]}\left(T_f - T_e\right) + C_pC_J\dfrac{dp}{dx} + \dfrac{v^2}{p}\dfrac{dp}{dx} - g\sin\theta\right\} \Big/ C_p \end{cases} \tag{C-7}$$

where ρ is the fluid density in kg/m^3; v is the fluid velocity in m/s; g is the gravity acceleration in m/s^2; θ is the deviation angle in °; f is the coefficient of friction resistance; p is the pressure in Pa; T_f is the temperature of fluid in wellbore in °C; T_e is the formation temperature in °C; C_p is the isobaric heat capacity in J/(kg·°C); C_J is the Joule-Thomson coefficient in °C/Pa; $f(t)$ is the dimensionless time function.

Affected by the thermal resistance of the tubing, annulus, casing and cement sheath, the wellbore fluid generates heat loss under different heat transfer coefficients during the radial heat transfer process to the surrounding formations (Hasan and Kabir, 2012). The expression of over-all heat-transfer coefficient is shown as

$$U_{to} = \left[\frac{r_{to}}{r_{ti}h_f} + \frac{r_{to}\ln(r_{to}/r_{ti})}{k_t} + \frac{1}{(h_{ac}+h_{ar})} + \frac{r_{to}\ln(r_{co}/r_{ci})}{k_c} + \frac{r_{to}\ln(r_h/r_{co})}{k_m}\right]^{-1} \tag{C-8}$$

where U_{to} is the over-all heat-transfer coefficient in J/(s·m^2·°C); r_{to} and r_{ti} are the outer and inner radius of tubing in m, respectively; h_f is the transfer coefficient of fluid in tubing J/(s·m^2·°C); h_{ac} is the transfer coefficient of annulus fluid in J/(s·m^2·°C); h_{ar} is the radiative heat transfer coefficient; k_t is the thermal conductivity of tubing; k_c is the thermal conductivity of casing; k_m is the thermal conductivity of cement sheath.

References

Chu, S., Zhang, L., Fan, J., et al., 2009. Experimental study of casing wear under impact-sliding conditions. Petrol. Sci. 6 (4), 445–450. https://doi.org/10.1007/s12182-009-0068-y.

Chen, F., Yan, S., Ye, H., et al., 2017. Double circular arc model based on average shear stress yield criterion and its application in the corroded pipe burst. J. Pet. Sci. Eng. 149, 515–521. https://doi.org/10.1016/j.petrol.2016.11.001.

Chen, S., Wang, H., Wang, Y., et al., 2020. Residual mechanical strength evaluation of corroded tubing in cryogenic carbon dioxide injection wellbore. J. Pet. Sci. Eng., 107398 https://doi.org/10.1016/j.petrol.2020.

Chen, S., Wang, H., Jiang, H., et al., 2021. Risk assessment of corroded casing based on analytic hierarchy process and fuzzy comprehensive evaluation. Petrol. Sci. 18 (2), 591–602. https://doi.org/10.1007/s12182-020-00507-0.

Gutman, E., 1994. Mechanochemistry of Solid Surface. World Scientific Publica-tion, Singapore.
De Waard, C., Lotz, U., Milliams, D.E., 1991. Predictive model for CO_2 corrosion engineering in wet natural gas pipelines. Corrosion 47 (12), 976–985. https://doi.org/10.5006/1.3585212.
Gao, D., Sun, L., Lian, J., 2010. Prediction of casing wear in extended reach drilling. Petrol. Sci. 7 (4), 494–501. https://doi.org/10.1007/S12182-001-0098-6.
Hou, D., Zeng, D., Shi, T., et al., 2013. The effects of sulfide stress cracking on the mechanical properties and intergranular cracking of P110 casing steel in sour environments. Petrol. Sci. 10 (3), 385–394. https://doi.org/10.1007/s12182-013-0286-1.
Huang, W., Zhang, X., Gao, D., et al., 2021. Casing wear shape and depth calculation model in a compound mode. Acta Pet. Sin. 42 (10), 1373–1381. https://doi.org/10.7623/syxb202110011 (in Chinese).
Hasan, A., Kabir, C., 2012. Wellbore heat-transfer modeling and applications. J. Pet. Sci. Eng. 86 (87), 127–136. https://doi.org/10.1016/j.petrol.2012.03.021.
Hasan, A., Kabir, C., Wang, X., 1998. Wellbore two-phase flow and heat transfer during transient testing. SPE J. 3 (2), 174–180. https://doi.org/10.2118/38946-PA.
Jin, C., Feng, F., F, F., 2020. Effect of variable drill pipe sizes on casing wear collapse strength. J. Pet. Sci. Eng. 195, 107856. https://doi.org/10.1016/j.petrol.2020.107856.
Liu, H., Dai, Y., Cheng, Y., 2019. Corrosion of underground pipelines in clay soil with varied soil layer thicknesses and aerations. Arabian Chemi 13, 3601–3614. https://doi.org/10.1016/j.arabjc.2019.11.006.
Lin, T., Zhang, Q., Lian, Z., et al., 2016. Evaluation of casing integrity defects considering wear and corrosion: application to casing design. J. Nat. Gas Sci. Eng. 29, 440–452. https://doi.org/10.1016/j.jngse.2016.01.029.
Li, H., Liu, Y., 2020. Petroleum Tubular Goods Engineering. Petroleum Industry Press, Beijing, pp. 345–347.
Qin, G., Cheng, Y., 2021. A review on defect assessment of pipelines: princip-les, numerical solutions, and applications. Int. J. Pres. Ves. Pip. 191, 104329. https://doi.org/10.1016/j.ijpvp.2021.104329.
Qian, S., Cheng, Y., 2019. Corrosion of X52 steel under thin layers of water condensate in wet gas pipelines. J. Nat. Gas Sci. Eng. 68, 102921. https://doi.org/10.1016/j.jngse.2019.102921.
Sun, J., Cheng, Y., 2019. Investigation by numerical modeling of the mechano-electrochemical interaction of circumferentially aligned corrosion defects on pipelines. Thin-Walled Struct. 144, 106314. https://doi.org/10.1016/j.tws.2019.106314.
Sun, J., Cheng, Y., 2020. Modelling of mechano-electrochemical interaction at overlapped corrosion defects and the implication on pipeline failure prediction. Eng. Fail. Anal. 212, 110466. https://doi.org/10.1016/j.engstruct.2020.110466.
Shi, X., Gao, D., Wang, Y., 2018. Predictive analysis on borehole temperature and pressure of HTHP gas wells considering coupling effect. Oil Drill & Pro Tec. 40 (5), 541–546. https://doi.org/10.13639/j.odpt.2018.05.001 (in Chinese).
Teigland, A., Dale, S., Sangesland, S., et al., 2021. A generalized empirical expression for the collapse of worn tubulars with a crescent-shaped wear groove under combined loads. J. Pet. Sci. Eng. 208, 109–187. https://doi.org/10.1016/j.petro.2021.109187.
White, J., Dawson, R., 1987. Casing wear: laboratory measurements and field predictions. SPE Drill. Eng. 2 (1), 56–62.. https://doi.org/10.2118/14325-PA.
Wang, T., Yan, X., Wang, J., et al., 2013. Investigation of the ultimate residual strengthen of a worn casing by using the Arc-Length algorithm. Eng. Fail. Anal. 28, 1–15. https://doi.org/10.1016/j.engfailanal.2012.09.008.
Wang, H., Yu, Y., Xu, W., et al., 2021. Time-variant burst strength of pipe with corrosion defects considering mechano-electrochemical interaction. Thin-Walled Struct. 169, 108479. https://doi.org/10.1016/j.tws.2021.108479.
Wu, J., Zhang, M., 2005. Casing burst strength after casing wear. In: SPE Conference. SPE-94304-MS. https://doi.org/10.2118/94304-MS.
Timoshenko, S.P., Goordier, J.N., 1972. Theory of Elasticity. McGraw-Hill, New York, pp. 196–202.
Yan, Y., Shao, B., Zhou, X., et al., 2019. A study on the influence of double ellipsoidal pitting corrosion on the collapsing strength of the casing. Eng. Fail. Anal. 100, 11–24. https://doi.org/10.1016/j.engfailanal.2019.02.020.
Yang, S., Yang, H., Liu, G., et al., 2016. Approach for fatigue damage assessment of welded structure considering coupling effect between stress and corrosion. Int. J. Fatig. 88, 88–95. https://doi.org/10.1016/j.ijfatigue.2016. 03.024.
Zhu, X., Liu, B., 2018. The reliability-based evaluation of casing collapsing st-rength and its application in marine gas reservoirs. Eng. Fail. Anal. 85, 1–13. https://doi.org/10.1016/j.engfailanal.2017.12.005.
Zhang, Q., Lian, Z., Lin, T., 2020. Prediction of residual burst strength of worn casing by theoretical and numerical modelling. Int. J. Pres. Ves. Pip. 188, 104195. https://doi.org/10.1016/j.ijpvp.2020.104195.
Zhang, Z., Li, J., Zheng, Y., et al., 2018. Finite service life evaluation method of production casing for sour-gas wells. J. Pet. Sci. Eng. 165, 171–180. https://doi.org/10.1016/j.petrol.2018.02.028.
Zeng, S., Song, B., Zeng, F., et al., 2021. Analysis of corrosion failure and materials selection for CO_2-H_2S gas well. J. Nat. Gas Sci. Eng. 86 (8), 103734. https://doi.org/10.1016/j.jngse.2020.103734.
Zhang, S., Zhou, W., 2021. Development of a burst capacity model for corroded pipelines considering corrosion defect width and a revised Folias factor equation. J. Nat. Gas Sci. Eng. 2, 103812. https://doi.org/10.1016/j.jngse.2021.103812.
Zhang, Z., Liu, Z., Xie, H., et al., 2017. Influence of shaft load-corrosion cou-pling on the service life of carbon steel casing pipe. Acta Pet. Sin. 38 (3), 342–347. https://doi.org/10.27643/syxb201703011 (in Chinese).
Zhang, X., Huang, W., Gao, D., 2022. Prediction model of casing wear shape and residual strength under compound modes. SPE J. 27 (4), 2183–2207.